

Observation of spin-glass behavior in 1111-type magnetic semiconductor (La, Ba)(Zn, Mn)SbO

Xueqin Zhao(赵雪芹), Jinou Dong(董金瓯), Rufei Zhang(张茹菲), Qiaolin Yang(杨巧林), Lingfeng Xie(谢玲凤), Licheng Fu(傅立承), Yilun Gu(顾轶伦), Xun Pan(潘洵), and Fanlong Ning(宁凡龙)
Citation: Chin. Phys. B, 2023, 32 (**12**): 127502. DOI: 10.1088/1674-1056/acf44a
Journal homepage: http://cpb.iphy.ac.cn; http://iopscience.iop.org/cpb

What follows is a list of articles you may be interested in

Li_2NiSe_2: A new-type intrinsic two-dimensional ferromagnetic semiconductor above 200 K

Li-Man Xiao(肖丽蔓), Huan-Cheng Yang(杨焕成), and Zhong-Yi Lu(卢仲毅)
Chin. Phys. B, 2023, 32 (**3**): 037501. DOI: 10.1088/1674-1056/aca39f

Gd impurity effect on the magnetic and electronic properties of hexagonal Sr ferrites: A case study by DFT

Masomeh Taghipour, Mohammad Yousefi, Reza Fazaeli, Masoud Darvishganji
Chin. Phys. B, 2020, 29 (**7**): 077505. DOI: 10.1088/1674-1056/ab8d9f

Progress of novel diluted ferromagnetic semiconductors with decoupled spin and charge doping: Counterparts of Fe-based superconductors

Shengli Guo(郭胜利), Fanlong Ning(宁凡龙)
Chin. Phys. B, 2018, 27 (**9**): 097502. DOI: 10.1088/1674-1056/27/9/097502

Study of magnetic and optical properties of $Zn_{1-x}TM_xTe$ (*TM*=Mn, Fe, Co, Ni) diluted magnetic semiconductors: First principle approach

Q Mahmood, M Hassan, M A Faridi
Chin. Phys. B, 2017, 26 (**2**): 027503. DOI: 10.1088/1674-1056/26/2/027503

Structural stability at high pressure, electronic, and magnetic properties of BaFZnAs: A new candidate of host material of diluted magnetic semiconductors

Bi-Juan Chen(陈碧娟), Zheng Deng(邓正), Xian-Cheng Wang(望贤成), Shao-Min Feng(冯少敏), Zhen Yuan(袁真), Si-Jia Zhang(张思佳), Qing-Qing Liu(刘清青), Chang-Qing Jin(靳常青)
Chin. Phys. B, 2016, 25 (**7**): 077503. DOI: 10.1088/1674-1056/25/7/077503

Observation of spin-glass behavior in 1111-type magnetic semiconductor (La, Ba)(Zn, Mn)SbO

Xueqin Zhao(赵雪芹)[1], Jinou Dong(董金瓯)[1], Rufei Zhang(张茹菲)[1], Qiaolin Yang(杨巧林)[1], Lingfeng Xie(谢玲凤)[1], Licheng Fu(傅立承)[1], Yilun Gu(顾轶伦)[1], Xun Pan(潘洵)[1], and Fanlong Ning(宁凡龙)[1,2,3,4,†]

[1] *Zhejiang Province Key Laboratory of Quantum Technology and Device and School of Physics, Zhejiang University, Hangzhou* 310027, *China*
[2] *State Key Laboratory of Silicon and Advanced Semiconductor Materials, Zhejiang University, Hangzhou* 310027, *China*
[3] *Collaborative Innovation Center of Advanced Microstructures, Nanjing University, Nanjing* 210093, *China*
[4] *Science and Technology Innovation Center, Chifeng High-Tech Industrial Development Zone, Chifeng* 025250, *China*

(Received 17 June 2023; revised manuscript received 18 August 2023; accepted manuscript online 28 August 2023)

We report the successful fabrication of a new 1111-type bulk magnetic semiconductor (La,Ba)(Zn,Mn)SbO through the solid solution of (La,Ba) and (Zn,Mn) in the parent compound LaZnSbO. The polycrystalline samples (La,Ba)(Zn,Mn)SbO crystallize into ZrCuSiAs-type tetragonal structure, which has the same structure as iron-based superconductor $LaFeAsO_{1-\delta}$. The DC magnetization measurements indicate the existence of spin-glass ordering, and the coercive field is up to $\sim$ 11500 Oe (1 Oe = 79.5775 A·m^{-1}). The AC magnetic susceptibility further determines that the samples evolve into a conventional spin-glass ordering state below the spin freezing temperature T_f. In addition, the negative magnetoresistance ($MR \equiv [\rho(H) - \rho(0)]/\rho(0)$) reaches -88% under 9 T.

Keywords: magnetic semiconductors, spin-glass, negative magnetoresistance

PACS: 75.50.Pp, 75.50.Lk, 75.30.Cr **DOI:** 10.1088/1674-1056/acf44a

1. Introduction

The research of spintronics is devoted to manipulating both charge and spin freedom of electrons.[1–3] As an important branch in spintronics, magnetic semiconductors (MSs) provide a new perspective for the preparation of novel electronics devices. III–V MS (Ga,Mn)As is the most well-investigated system,[4] which is more compatible with optoelectronic devices applied in industry. In the mid-1990s, the fabrication of (Ga,Mn)As films made significant progress via low temperature molecular beam epitaxy (LT-MBE) method. With the injection of spin-polarized carriers, (Ga,Mn)As provides a new choice for the preparation of multifunctional heterojunctions with non-magnetic semiconductor GaAs. For example, Ohno *et al*. has successfully prepared spin-polarized light-emitting diode (Spin-LED) based on (Ga,Mn)As.[5] At present, the Curie temperature (T_C) of (Ga,Mn)As has reached $\sim$ 190 K–200 K,[6,7] which is still below room temperature. Moreover, the inequivalent substitutions of (Ga^{3+}, Mn^{2+}) introduce carriers and magnetic moments simultaneously, which makes it difficult to control carrier densities and magnetic moments independently. In addition, the MBE method is a non-equilibrium growth method, which makes the properties of materials sensitive to the growth conditions and may cause defects during the growth process. These challenges have aroused great interest in exploring more novel MSs, if possible, with higher T_C.

In recent years, several series of bulk Zn-based MSs with decoupled carrier and spin doping have been reported, including 111-type Li(Zn,Mn)As,[8] Li(Cd,Mn)P,[9] 122-type (Ba,K)(Zn,Mn)$_2$As$_2$,[10] (Ca,Na)(Zn,Mn)$_2$ Sb$_2$,[11] 1111-type (La,Ba)(Zn,Mn)AsO,[12] La(Zn,Mn,Cu)SbO,[13] 2114-type Cu$_2$(Zn,Mn)(Sn,Al)Se$_4$.[14] The equivalent substitutions of (Zn^{2+},Mn^{2+}) result in higher chemical solubility of magnetic atoms, compared with III–V MSs. The T_C of (Ba,K)(Zn,Mn)$_2$As$_2$ has reached $\sim$ 230 K,[15] which is already higher than that of (Ga,Mn)As. On the other hand, bulk semiconductor materials enable the measurements of microscopic probes, such as neutron scattering, nuclear magnetic resonance (NMR) and muon spin relaxation (μSR),[10,12,16] which has demonstrated that these bulk MSs share the same mechanism of ferromagnetic ordering as that of (Ga,Mn)As.

Unlike the magnetic semiconductors mentioned above, which can exhibit long-range ferromagnetic ordering, some magnetic semiconductors exhibit spin-glass behavior.[17] Back to 1980's, when doping Mn into II–VI semiconductors such as ZnTe and HgTe, spin-glass ordering states had been usually observed in (Zn,Mn)Te[18] and (Hg,Mn)Te.[19] The reason is that the iso-valent substitution of Zn or Hg by Mn only introduces magnetic moments, and there are no enough carriers to build up the long-range ferromagnetic ordering. On the other hand, in some recently reported bulk form MSs, such as Ba(Zn,Mn,Cu)$_2$As$_2$[20] and Na(Zn,Mn)Sb,[21] spin-glass ordering state or glassy ferromagnetism has also been observed. These spin-glass state could be ascribed to the magnetic frus-

†Corresponding author. E-mail: ningfl@zju.edu.cn

© 2023 Chinese Physical Society and IOP Publishing Ltd

tration generated by the competition between the indirect ferromagnetic and direct antiferromagnetic interactions.

As a valuable method in the study of magnetic condensed materials, pressure has been extensively applied to explore the mechanism of magnetic interactions, especially in magnetic semiconductors where ferromagnetic interactions are mediated by carriers. At present, the effect of physical pressure and chemical pressure on ferromagnetism in MSs has been widely studied. For example, in traditional III–V MS (In,Mn)Sb, T_C has increased by 25% under a hydrostatic pressure of 2.7 GPa.[22] In addition, in n-type MS Ba(Zn,Co)$_2$As$_2$, the substitutions of (Ba,Sr) and (As,Sb) introduce positive and negative chemical pressure, respectively, and it was found that negative chemical pressure reduced T_C, while positive chemical pressure increased T_C by 18%.[23] Previously, starting from the narrow band-gap semiconductor LaZnSbO, MSs (La,Ca)(Zn,Mn)SbO[24] and (La,Sr)(Zn,Mn)SbO[25] with the maximum $T_C \sim 40$ K and ~ 27 K have been reported. We note that for the same doping level, T_C is ~ 20 K for (La$_{0.95}$Ca$_{0.05}$)(Zn$_{0.95}$Mn$_{0.05}$)SbO, while T_C is ~ 14 K for (La$_{0.95}$Sr$_{0.05}$)(Zn$_{0.95}$Mn$_{0.05}$)SbO. This is largely because the ionic radius of Sr^{2+} is larger than that of Ca^{2+}, that is, negative chemical pressure suppresses T_C.

In this paper, we attempt to synthesize (La, Ba)(Zn, Mn)SbO, and explore how chemical pressure will affect the magnetic properties in whole (La,*AE*)(Zn,Mn)SbO (*AE* = Ca, Sr, Ba) system. The substitutions of (La^{3+},Ba^{2+}) and (Zn^{2+},Mn^{2+}) in the parent compound LaZnSbO introduce carriers and local magnetic moments, respectively. Next, we fix the doping level x of Ba^{2+} at 0.05 and change the amount of magnetic atoms Mn, and explore how the spin densities affect magnetism in (La$_{0.95}$Ba$_{0.05}$)(Zn$_{1-x}$Mn$_x$)SbO ($x = 0.025$, 0.05, 0.075, 0.10). The DC magnetization measurements show the presence of short-range ferromagnetic correlations in our specimens. The AC magnetic susceptibility measurements demonstrate that (La,Ba)(Zn,Mn)SbO exhibits the characteristics of spin-glass ordering state below spin freezing temperature T_f, rather than long-range ferromagnetic ordering as in (La,Ca)(Zn,Mn)SbO and (La,Sr)(Zn,Mn)SbO. A local maximum of resistance and negative magnetoresistance under an applied magnetic field have been observed, resulting from multiple interactions between quantum localization and carrier correlations.[26] With more Mn doping, resistivity increases significantly, which is attributed to the scattering of carriers caused by magnetic fluctuations.

2. Experiments

Polycrystalline samples (La$_{0.95}$Ba$_{0.05}$)(Zn$_{1-x}$Mn$_x$)SbO ($x = 0.025$, 0.05, 0.075, 0.10) were prepared through the solid-state reaction method. First of all, high-purity La (99.9%, Alfa Aesar), Ba (99.2%, Alfa Aesar), Zn (99.9%, Alfa Aesar), MnO (99.5%, Aladdin), and Sb (99.999%, Prmat) were mixed according to the nominal composition. The mixtures were placed in the aluminum crucibles, sealed in evacuated silica tubes, then heated to 900 °C and kept for 24 h. The precursors were fully grounded and pressed into pellets with 8 mm in diameter, then placed in aluminum crucibles, and sealed in evacuated silica tubes. Subsequently, the pellets were heated to 1100 °C and kept for 40 h. All procedures except evacuating silica tubes are conducted in a glove box filled with high-purity argon.

To determine the crystal structure of polycrystalline samples LaZnSbO and (La$_{0.95}$Ba$_{0.05}$)(Zn$_{1-x}$Mn$_x$)SbO ($x = 0.025$, 0.05, 0.075, 0.10), the powder x-ray diffraction was carried out by a powder x-ray diffractometer (Model EMPYREAN) with monochromatic Cu-$K_{\alpha 1}$ radiation. The lattice parameters were calculated by Rietveld refinements using open-source GSAS-II package.[27] The DC magnetization was measured on a Quantum Design magnetic property measurement system (MPMS-3). The AC magnetic susceptibility and magnetoresistance were measured on a Quantum Design physical property measurement system (PPMS). Four-probe technique was applied to the measurements of electrical resistivity.

3. Results and discussion

We show the x-ray diffraction patterns in the 2θ range of 10°–100° for polycrystalline samples LaZnSbO and (La$_{0.95}$Ba$_{0.05}$) (Zn$_{1-x}$Mn$_x$)SbO ($x = 0.025$, 0.05, 0.075, 0.10) in Fig. 1(a). The diffraction peaks are consistent with a ZrCuSiAs-type tetragonal structure (space group $P4/nmm$), as shown in the inset of Fig. 1(b). The Rietveld refinement for (La$_{0.95}$Ba$_{0.05}$)(Zn$_{0.95}$Mn$_{0.05}$)SbO is plotted in Fig. 1(b). The resultant weighted reliable factor R_{wp} is 7.189%, indicating that the samples are in good quality. LaZnSbO share the same structure as that of the direct-gap semiconductor LaZnAsO[28] and Fe-based layered superconductor LaFeAsO$_{1-\delta}$.[29] The structure of LaZnSbO can be described as the stacking of $[LaO]^+$ layers and $[ZnSb]^-$ layers along c axis.[30] A few small peaks (marked as $*$) are observed in some samples. These are non-magnetic impurities ZnSb, and will not affect the discussion of magnetism in the following.

The calculated lattice parameters a and c of parent compound LaZnSbO are 4.2285 Å and 9.5414 Å, respectively, which is close to previously reported values $a = 4.2260$ Å and $c = 9.5369$ Å.[31] In Fig. 1(c), we can see that the lattice parameters a and c of (La$_{0.95}$Ba$_{0.05}$)(Zn$_{1-x}$Mn$_x$)SbO ($x = 0.025$, 0.05, 0.075, 0.10) monotonically increase with the increasing of Mn doping, which is due to the fact that the ionic radius of Mn^{2+} is larger than that of Zn^{2+}. Obviously, with the Mn doping level increasing, the unit cell volume also increases monotonically, as shown in Fig. 1(d). These provide strong evidences for the successful solution of (La^{3+},Ba^{2+}) and (Zn^{2+},Mn^{2+}).

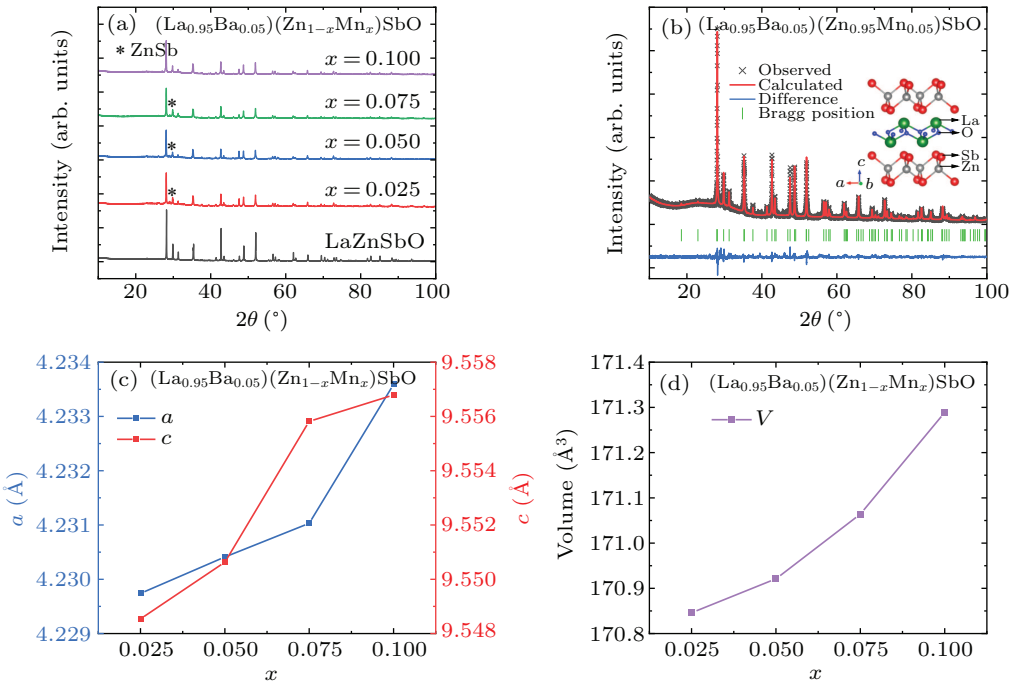


Fig. 1. (a) The powder x-ray diffraction patterns for polycrystals LaZnSbO and $(La_{0.95}Ba_{0.05})(Zn_{1-x}Mn_x)SbO$ ($x = 0.025$, 0.05, 0.075, 0.10). The stars (∗) represent the traces of impurities ZnSb. (b) The Rietveld refinement for $(La_{0.95}Ba_{0.05})(Zn_{0.95}Mn_{0.05})SbO$. Inset is the crystal structure of parent compound LaZnSbO. (c) The lattice parameters a and c obtained from the Rietveld refinements for $(La_{0.95}Ba_{0.05})(Zn_{1-x}Mn_x)SbO$ ($x = 0.025$, 0.05, 0.075, 0.10). (d) The unit cell volume (V) versus doping level x for $(La_{0.95}Ba_{0.05})(Zn_{1-x}Mn_x)SbO$ ($x = 0.025$, 0.05, 0.075, 0.10).

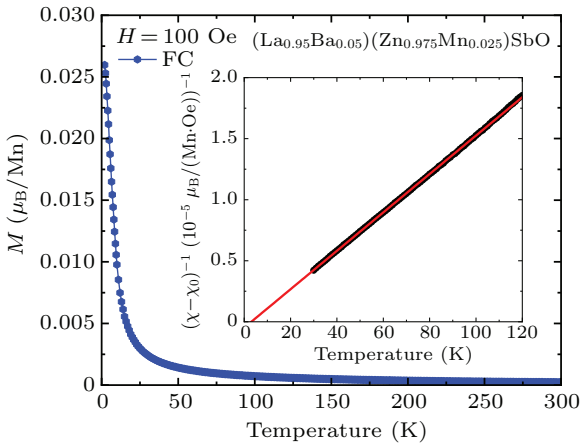


Fig. 2. The temperature dependence of DC magnetization M of $(La_{0.95}Ba_{0.05})(Zn_{0.975}Mn_{0.025})SbO$ under field-cooling condition in an external field $H_{ext} = 100$ Oe. Inset is the plot of $1/(\chi - \chi_0)$ versus temperature. The black solid circles are the data, and the red straight line is a linear fitting of the Curie–Weiss law.

In Fig. 2, we show the temperature dependence of DC magnetization (M) under field-cooling modes with the external field $H_{ext} = 100$ Oe for $(La_{0.95}Ba_{0.05})(Zn_{0.975}Mn_{0.025})SbO$. We did not observe obvious magnetic transition in the entire temperature range. We fit the data of high temperature region using the Curie–Weiss law and show it in the inset of Fig. 2. The obtained Weiss temperature (θ) is ~ 3.0 K. Positive θ indicates that the exchange interaction is ferromagnetic. However, this value is too small, we will not focus on $(La_{0.95}Ba_{0.05})(Zn_{0.975}Mn_{0.025})SbO$ in the following.

In Fig. 3(a), we show the temperature dependence of DC magnetization under zero-field-cooling (ZFC) and field-cooling (FC) modes in an applied field $H_{ext} = 100$ Oe for $(La_{0.95}Ba_{0.05})(Zn_{1-x}Mn_x)SbO$ ($x = 0.05$, 0.075, 0.10). Magnetization suddenly increases around 20 K–30 K. In addition, the magnetization under FC mode at the base temperature of 2 K, M_{base}, is ~ 0.020 μ_B/Mn for $x = 0.05$, then increases to 0.028 μ_B/Mn for $x = 0.075$, and decreases to 0.017 μ_B/Mn for $x = 0.10$. This probably arises from the competition between ferromagnetic and antiferromagnetic interactions among Mn atoms. The probability that two Mn atoms at the nearest-neighbor (NN) sites satisfies $P = C_4^1 x(1-x)^3$. For example, for the doping level of $x = 0.075$, the probability of finding one Mn atom at its NN sites is $P = C_4^1 \times 0.075 \times 0.925^3 = 23.74\%$, and P increases to 29.16% for $x = 0.10$. With the increasing of Mn atoms, the possibility of Mn atoms at the NN sites increases, which enhances antiferromagnetic interactions. That is, doping too many Mn atoms is detrimental to the ferromagnetic interactions.

For the purpose of quantifying the temperature of magnetic transition, we plot $dM(T)/dT$ versus T in Fig. 3(c). With the increasing of Mn doping, the minimum values of $dM(T)/dT$ (defined as T_{dif}) increase first and then decrease. On the other hand, we fit the magnetic susceptibility curves at the high temperature region using the Curie–Weiss law $\chi = \chi_0 + C/(T - \theta)$, C is the Curie constant related to the effective magnetic moment, χ_0 is a temperature-independent term, and θ is the Weiss temperature. The fitting results of $1/(\chi - \chi_0)$ versus temperature under FC mode are shown in Fig. 3(d). The Weiss temperatures θ are the intersections of the fitting lines with the x axis. θ is 8 K for $x = 0.05$, then increases to 19 K for $x = 0.075$, and decreases to 15 K for

$x = 0.10$. The positive values of the Weiss temperatures θ imply the establishment of ferromagnetic correlation between distant Mn atoms. We find that $T_{\rm dif}$ and θ have the same trend with the change of doping level x. That is, both increase at first and decrease afterwards with the increasing of Mn doping level x. This reflects that more Mn atoms suppress the ferromagnetic interactions, which is attributed to the competition between the short-range antiferromagnetic interactions among the NN Mn atoms and long-range ferromagnetic interactions induced by itinerant electrons.[32]

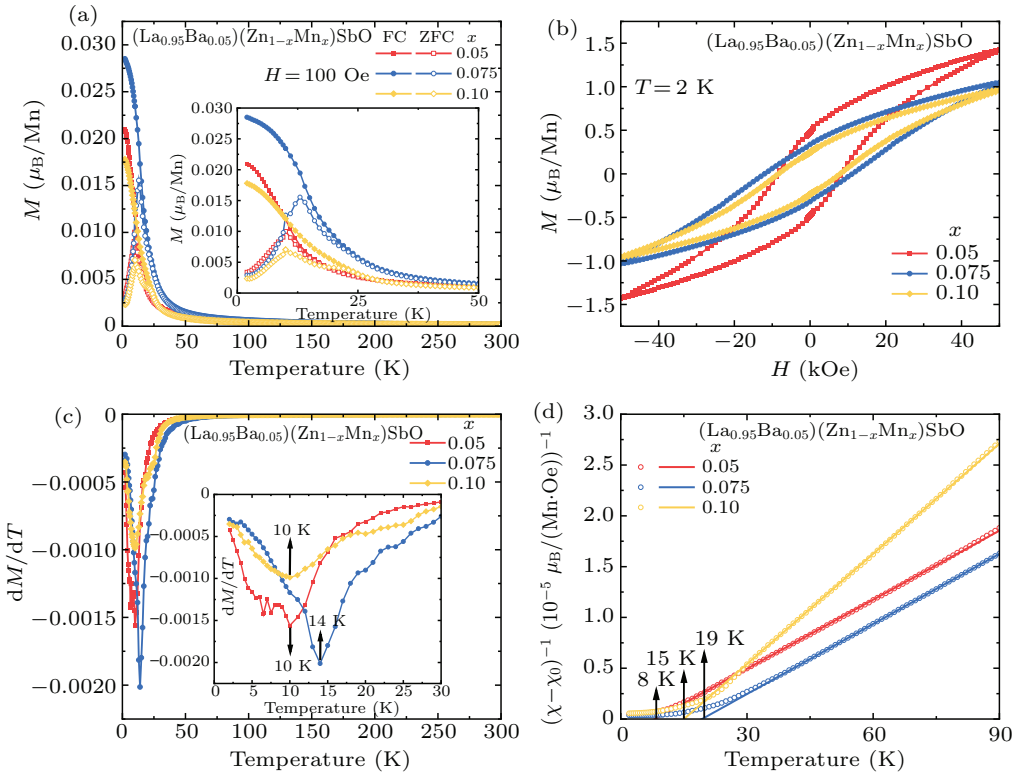


Fig. 3. (a) The temperature dependence of DC magnetization for $(La_{0.95}Ba_{0.05})(Zn_{1-x}Mn_x)SbO$ ($x = 0.05, 0.075, 0.10$) in zero-field-cooling (ZFC) and field-cooling (FC) modes with $H_{\rm ext} = 100$ Oe. Inset shows the enlarged $M(T)$ curves for $(La_{0.95}Ba_{0.05})(Zn_{1-x}Mn_x)SbO$ ($x = 0.05$, 0.075, 0.10). (b) The iso-thermal magnetization for $(La_{0.95}Ba_{0.05})(Zn_{1-x}Mn_x)SbO$ ($x = 0.05, 0.075, 0.10$) measured at 2 K. (c) The $dM(T)/dT$ versus T plots for $(La_{0.95}Ba_{0.05})(Zn_{1-x}Mn_x)SbO$ ($x = 0.05, 0.075, 0.10$). Inset shows an enlargement of 2 K to 30 K region, and arrows mark the position of the minimum values of $dM(T)/dT$. (d) The curves of $1/(\chi - \chi_0)$ versus T for $(La_{0.95}Ba_{0.05})(Zn_{1-x}Mn_x)SbO$ ($x = 0.05$, 0.075, 0.10). The lines represent the fitting of Curie–Weiss law, and arrows mark the Weiss temperatures θ.

We show the iso-thermal magnetization measured at 2 K for $(La_{0.95}Ba_{0.05})(Zn_{1-x}Mn_x)SbO$ ($x = 0.05$, 0.075, 0.10) in Fig. 3(b). Clear hysteresis can be observed, demonstrating the presence of ferromagnetic interactions. The coercive field ($H_{\rm C}$) is ~ 8400 Oe for $x = 0.05$, then increases to ~ 11500 Oe for $x = 0.075$, and decreases to ~ 8150 Oe for $x = 0.10$. We calculate the effective magnetic moment ($\mu_{\rm eff}$) by formula $C = N\mu_0\mu_{\rm eff}^2/3k_{\rm B}$. The obtained parameters are listed in Table 1.

Table 1. The minimum values ($T_{\rm dif}$) of $dM(T)/dT$, the Weiss temperature θ, the effective magnetic moment $\mu_{\rm eff}$, the base temperature moment $M_{\rm base}$, and the coercive field $H_{\rm C}$ for $(La_{0.95}Ba_{0.05})(Zn_{1-x}Mn_x)SbO$ ($x = 0.05, 0.075, 0.10$).

x	$T_{\rm dif}$ (K)	θ (K)	$\mu_{\rm eff}$ (μ_B/Mn)	$M_{\rm base}$ (μ_B/Mn)	$H_{\rm C}$ (Oe)
0.05	10	8	4.55	0.020	8400
0.075	14	19	4.40	0.028	11500
0.10	10	15	3.51	0.017	8150

The Arrot–Noakes plots[33,34] (M^2 versus H/M) obtained from iso-thermal magnetization at different temperatures for $(La_{0.95}Ba_{0.05})(Zn_{0.925}Mn_{0.075})SbO$ are displayed in Fig. 4. No indication of spontaneous magnetization is observed. Combined with the iso-thermal magnetization curves shown in Fig. 3(b), where magnetization is still not saturated with the external magnetic field up to 5 T, we can say that it is not a long-range ferromagnetic ordering but a short-range spin-glass ordering state.

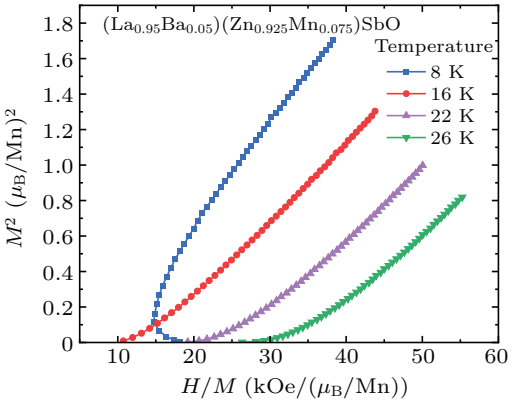


Fig. 4. The Arrott plots of $(La_{0.95}Ba_{0.05})(Zn_{0.925}Mn_{0.075})SbO$ under various temperatures.

To further determine whether the samples is in a spin-

glass ordering state, we conduct the AC magnetic susceptibility for $(La_{0.95}Ba_{0.05})(Zn_{0.925}Mn_{0.075})SbO$ under an external AC field amplitude of 10 Oe with different frequencies (f). The cusp positions of the real part χ' in Fig. 5(a) and the imaginary part χ'' in Fig. 5(b) are obviously frequency-dependent. With the increasing of frequency, the real part χ' and the imaginary part χ'' move towards the higher temperature region, and the magnitude reduces slightly. We define the cusp position of the real part χ' as the static spin freezing temperature (T_f). According to the formula $K = \Delta T_f/[T_f \Delta \log f]$,[35] we obtain the value of K in Fig. 5(c). The $K \sim 0.055$ is whin the range of canonical spin-glass system ($K \sim 0.005$–0.08),[36] this indicates that the samples exhibit a spin-glass ordering state below T_f. The random arrangement of Mn atoms in lattice induces not only ferromagnetic but also antiferromagnetic interactions among Mn atoms. Their competition induces the spin-glass ordering state. The similar behavior has also been observed in $Ba(Zn,Mn,Cu)_2As_2$.[20]

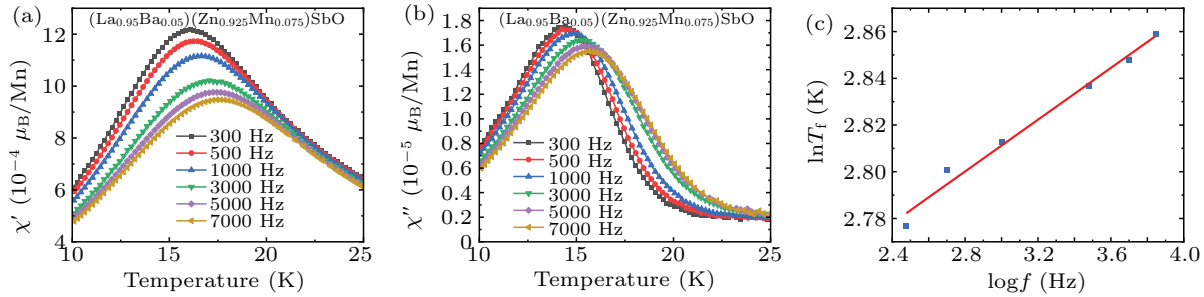


Fig. 5. The (a) real part χ' and (b) imaginary part χ'' of AC magnetic susceptibility for $(La_{0.95}Ba_{0.05})(Zn_{0.925}Mn_{0.075})SbO$ at different frequencies f. (c) The frequency dependence of spin freezing temperature T_f plotted as $\ln T_f$ versus $\log f$ for $(La_{0.95}Ba_{0.05})(Zn_{0.925}Mn_{0.075})SbO$.

We performed the electrical transport measurements on the parent compound LaZnSbO and doped samples $(La_{0.95}Ba_{0.05})(Zn_{1-x}Mn_x)SbO$ ($x = 0.025$, 0.05, 0.075, 0.10). The curves of the temperature-dependent electrical resistivity $\rho(T)$ are shown in Fig. 6(a). The parent compound LaZnSbO shows the semiconducting behavior, as shown in the inset of Fig. 6(a). After the solid solution of (La,Ba) and (Zn,Mn), resistivity $\rho(T)$ still retains the semiconducting behavior. On the other hand, with the increasing of the Mn-doped levels x, the magnitude of the resistivity increases significantly. This can be attributed to the scattering of carriers by spins at low temperatures.

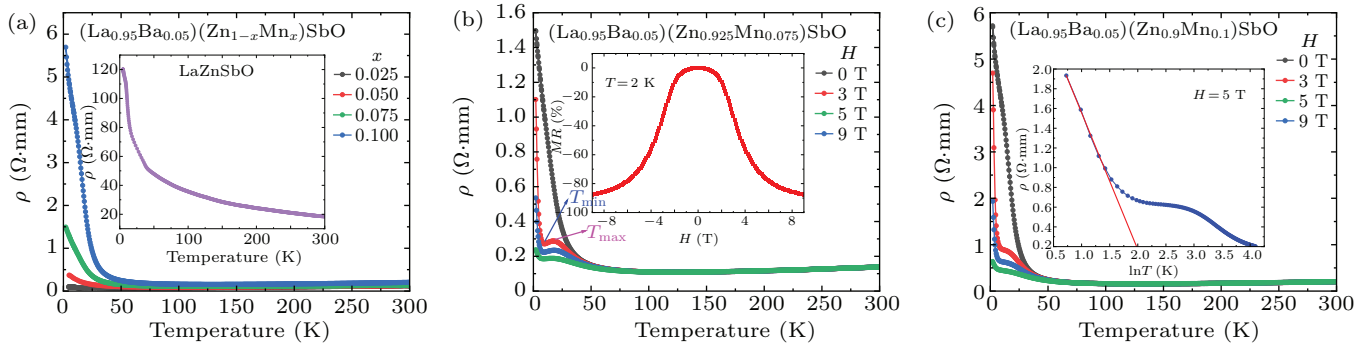


Fig. 6. (a) The temperature-dependent resistivity $\rho(T)$ for LaZnSbO (inset) and $(La_{0.95}Ba_{0.05})(Zn_{1-x}Mn_x)SbO$ ($x = 0.025$, 0.05, 0.075, 0.10). (b) The magnetoresistance for $(La_{0.95}Ba_{0.05})(Zn_{0.925}Mn_{0.075})SbO$ under the external field $H_{ext} = 0$ T, 3 T, 5 T, 7 T, 9 T. The inset shows the field dependence of magnetoresistance ($MR \equiv [\rho(H) - \rho(0)]/\rho(0)$) measured in an external field ranging from 0 T to −9 T and 0 T to 9 T at 2 K. (c) The magnetoresistance of $(La_{0.95}Ba_{0.05})(Zn_{0.9}Mn_{0.1})SbO$ with $H_{ext} = 0$ T, 3 T, 5 T, 7 T, 9 T. Inset shows resistivity $\rho(T)$ versus $\ln T$ under $H_{ext} = 5$ T.

In Fig. 6(b), we show the temperature-dependent magnetoresistance curves for $(La_{0.95}Ba_{0.05})(Zn_{0.925}Mn_{0.075})$ SbO under the field of 0 T, 3 T, 5 T, 7 T, 9 T, respectively. The resistivity is suppressed rapidly with the increasing of applied magnetic field, that is, the negative magnetoresistance occurs. As the temperature goes down, a local maximum of resistivity (as marked by T_{max} in Fig. 6(b)) occurs under an applied magnetic field. Similar phenomenon has been observed in many MSs, such as traditional III–V compound (Ga,Mn)As, and novel bulk materials $(Sr,Na)(Zn,Mn)_2As_2$[37] and $(Ba,K)(Cd,Mn)_2As_2$.[26] This field-induced insulator-to-metal transition is probably caused by multiple interactions between quantum localization and carrier correlations.[26] In (Ga,Mn)As system, the behavior of resistivity maximum near the Curie temperature T_C and associated negative magnetoresistance are ascribed to the existence of randomly oriented ferromagnetic bubbles, which drives efficient spin-disorder scattering of carriers, and thus reduces the anti-localization quantum corrections to conductivity.[38,39] Subsequently, as the temperature continues decreasing, a local minimum of resistance (as marked by T_{min} in Fig. 6(b)) occurs, followed by a strong upturn. The suppression of spin-dependent scattering

in an external magnetic field leads to large negative magnetoresistance ($MR \equiv [\rho(H) - \rho(0)]/\rho(0)$). As shown in the inset of Fig. 6(b), for $(La_{0.95}Ba_{0.05})(Zn_{0.925}Mn_{0.075})SbO$, the MR reaches up to -88% under 9 T. Such a colossal negative magnetoresistance MR has also been observed in spin-glass (Cd,Mn)Se.[17]

Compared with the doping level $x = 0.075$ in Fig. 6(b), when the doping level x increases to 0.1 as shown in Fig. 6(c), the magnitude of resistivity is lifted up. In the inset of Fig. 6(c), the resistivity for $(La_{0.95}Ba_{0.05})(Zn_{0.9}Mn_{0.1})SbO$ at low temperature under $H_{ext} = 5$ T linearly depends on $\ln T$, which mimics that of the Kondo effect.[40] This phenomenon could also be interpreted by quantum corrections to the conductivity in the weakly localized regime,[38,39,41] because spin polarization of carriers destroys the Kondo effect.[39]

4. Discussion and conclusion

The ionic radius of Ca^{2+}, Sr^{2+}, and Ba^{2+} are 0.99 Å, 1.13 Å, and 1.35 Å, respectively. Replacing La^{3+} with Ca^{2+}, Sr^{2+}, and Ba^{2+} respectively is expanding the lattice successively, which is equivalent to inducing negative chemical pressure into the system. Thus, the expansion of lattice causes Zn/Mn–Sb bond length to increase continuously, and p–d hybridization between local moments and hole carriers is weaken, which results in the suppression of ferromagnetic interactions.[42] Comparing the whole $(La_{0.95}AE_{0.05})(Zn_{0.95}Mn_{0.05})SbO$ (AE = Ca, Sr, Ba) system, the magnetization under FC mode at the base temperature of 2 K is ~ 0.60 μ_B/Mn for $(La_{0.95}Ca_{0.05})(Zn_{0.95}Mn_{0.05})SbO$, 0.15 μ_B/Mn for $(La_{0.95}Sr_{0.05})(Zn_{0.95}Mn_{0.05})SbO$, and reduces to 0.02 μ_B/Mn for $(La_{0.95}Ba_{0.05})(Zn_{0.95}Mn_{0.05})SbO$. On the other hand, as the ionic radius of AE ions increases, the Curie temperature T_C decreases from $\sim$ 20 K for $(La_{0.95}Ca_{0.05})(Zn_{0.95}Mn_{0.05})SbO$ to 14 K for $(La_{0.95}Sr_{0.05})(Zn_{0.95}Mn_{0.05})SbO$, and no long-range ordering is formed in $(La_{0.95}Ba_{0.05})(Zn_{0.95}Mn_{0.05})SbO$. Furthermore, in the same 1111-type (La,Ba)(Zn,Mn)AsO MS, μSR measurements indicate that ferromagnetic ordering develops in the entire volume.[12] While for (La,Ba)(Zn,Mn)SbO, the ionic radius of Sb^{3-} (2.45 Å) is larger than that of As^{3-} (2.22 Å), which leads to the result that the bond length of Zn/Mn–Sb is larger than that of Zn/Mn–As. Therefore, the p–d hybridization in (La,Ba)(Zn,Mn)SbO is much weaker, which eventually develops into spin-glass ordering state. We should note that in both (La,Ba)(Zn,Mn)AsO and (La,Ba)(Zn,Mn)SbO, carriers are coming from the substitutions of Ba for La which takes place in the La–O layers. While in another 1111-type La(Zn,Mn,Cu)SbO compound, the substitutions of Mn and Cu for Zn are taking place in the same Zn–Sb layers where the holes induced by Cu substitutions for Zn mediate the magnetic moments arising from Mn substitutions for Zn.

To summarize, we successfully synthesized a new 1111-type bulk MS (La,Ba)(Zn,Mn)SbO. The DC magnetization measurements reveal that the ferromagnetic interactions increase initially and then decrease with more Mn atoms doping, and the coercive field H_C is as high as $\sim$ 11500 Oe. According to the AC magnetic susceptibility measurements, the samples evolve into conventional spin-glass ordering state below the spin freezing temperature T_f. The negative magnetoresistance MR for $x = 0.075$ has reached -88% at 2 K under the applied field of 9 T. We note that spin-glass ground state is common in II–VI MSs, and not unusual in recent bulk form MSs with decoupled charge and spin doping. The reason is largely ascribed to the strength of magnetic interactions and the competition between the long-range indirect ferromagnetic interactions of remote spins and the short-range direct antiferromagnetic interactions of moments at the NN sites. To understand the general mechanism for the ferromagnetic ordering in all magnetic semiconductors, this physical phenomenon has to be considered as an important part for the whole picture. Our sample enriches the MS families and is helpful for searching new MS materials with high T_C. Furthermore, (La,Ba)(Zn,Mn)SbO has the same ZrSiCuAs-type tetragonal structure and favorable lattice matching as Fe-based layered superconductor LaFeAsO,[29] and it is possible to benefit potential spintronics applications.

Acknowledgements

Project supported by the National Key Research and Development Program of China (Grant Nos. 2022YFA1402701 and 2022YFA1403202), the National Natural Science Foundation of China (Grant No. 12074333), and the Key Research and Development Program of Zhejiang Province, China (Grant No. 2021C01002).

References

[1] Žutić I, Fabian J and Sarma S D 2004 *Rev. Mod. Phys.* **76** 323
[2] Wolfand S A, Awschalom D D, Buhrman R A, Daughton J M, von Molnár S, Roukesand M L, Chtchelkanova A Y and Treger D M 2001 *Science* **294** 1488
[3] Dietl T and Ohno H 2014 *Rev. Mod. Phys.* **86** 187
[4] Ohno H 1998 *Science* **281** 951
[5] Ohno Y, Young D K, Beschoten B, Matsukura F, Ohno H and Awschalom D D 1999 *Nature* **402** 790
[6] Chen L, Yan S, Xu P F, Lu J, Wang W Z, Deng J J, Qian X, Ji Y and Zhao J H 2009 *Appl. Phys. Lett.* **95** 182505
[7] Chen L, Yang X, Yang F H, Zhao J H, Misuraca J, Xiong P and von Molnár S 2011 *Nano Lett.* **11** 2584
[8] Deng Z, Jin C Q, Liu Q Q, Wang X C, Zhu J L, Feng S M, Chen L C, Yu R C, Arguello C, Goko T, Ning F L, Zhang J S, Wang Y Y, Aczel A A, Munsie T, Williams T J, Luke G M, Kakeshita T, Uchida S, Higemoto W, Ito T U, Gu B, Maekawa S, Morris G D and Uemura Y J 2011 *Nat. Commun.* **2** 422
[9] Han W, Chen B J, Gu B, Zhao G Q, Yu S, Wang X C, Liu Q Q, Deng Z, Li W M, Zhao J F, Cao L P, Peng Y, Shen X, Zhu X H, Yu R C, Maekawa S, Uemura Y J and Jin C Q 2019 *Sci. Rep.* **9** 7490

[10] Zhao K, Deng Z, Wang X C, Han W, Zhu J L, Li X, Liu Q Q, Yu R C, Goko T, Frandsen B, Liu L, Ning F L, Uemura Y J, Dabkowska H, Luke G M, Luetkens H, Morenzoni E, Dunsiger S R, Senyshyn A, Böni P and Jin C Q 2013 *Nat. Commun.* **4** 1442

[11] Gu Y L, Zhang H J, Zhang R F, Fu L C, Wang K, Zhi G X and Guo S L and Ning F L 2020 *Chin. Phys. B* **29** 057507

[12] Ding C, Man H Y, Qin C, Lu J C, Sun Y L, Wang Q, Yu B Q, Feng C M, Goko T, Arguello C J, Liu L, Frandsen B A, Uemura Y J, Wang H D, Luetkens H, Morenzoni E, Han W, Jin C Q, Munsie T, William T J, D'Ortenzio R M, Medina T, Luke G M, Imai T and Ning F L 2013 *Phys. Rev. B* **88** 041102

[13] Zhao Y, Wang K, Guo S L, Fu L C, Gu Y L, Zhi G X, Xu L X, Cui Q, Cheng J G, Wang H D, Chen B and Ning F L 2018 *Europhys. Lett.* **120** 47005

[14] Zhi G X, Guo S L, Zhang R F, Zhao Y, Fu L C, Gu Y L, Wang K, Zhang H J, Zhao X Q, Dong J O, Xie L F and Ning F L 2021 *J. Magn. Magn. Mater.* **536** 168064

[15] Zhao K, Chen B J, Zhao G Q Yuan Z, Liu Q Q, Deng Z, Zhu J L and Jin C Q 2014 *Chin. Sci. Bull.* **59** 2524

[16] Ding C, Qin C, Man H Y, Imai T and Ning F L 2013 *Phys. Rev. B* **88** 041108

[17] Furdyna J K 1988 *J. Appl. Phys.* **64** R29

[18] McAlister S P, Furdyna J K and Giriat W 1984 *Phys. Rev. B* **29** 1310

[19] Nagata S, Galazka R R, Mullin D P, Akbarzadeh H, Khattak G D, Furdyna J K and Keesom P H 1980 *Phys. Rev. B* **22** 3331

[20] Man H Y, Guo S L, Sui Y, Guo Y, Chen B, Wang H D, Ding C and Ning F L 2015 *Sci. Rep.* **5** 15507

[21] Yu S, Peng Y, Zhao G Q, Zhao J F, Wang X C, Zhang J, Deng Z and Jin C Q 2023 *J. Semicond* **44** 032501

[22] Csontos M, Mihaly G, Jankó B, Wojtowicz T, Liu X and Furdyna J K 2005 *Nat. Mater.* **4** 447

[23] Fu L C, Gu Y L, Zhi G X, Zhang H J, Zhang R F, Dong J O, Zhao X Q, Xie L F and Ning F L 2021 *Sci. Rep.* **11** 7652

[24] Han W, Zhao K, Wang X C, Liu Q Q, Ning F L, Deng Z, Liu Y, Zhu J L, Ding C, Man H Y and Jin C Q 2013 *Sci. China-Phys. Mech. Astron.* **56** 2026

[25] Zhang H J, Zhang R F, Fu L C, Gu Y L, Zhi G X, Dong J O, Zhao X Q and Ning F L 2021 *Acta Phys. Sin.* **70** 107501 (in Chinese)

[26] Yang X J, Li Y K, Zhang P, Jiang H, Luo Y K, Chen Q, Feng C M, Cao C, Dai J H, Tao Q, Cao G H and Xu Z A 2013 *J. Appl. Phys.* **114** 223905

[27] Toby B H and Von Dreele R B 2013 *J. Appl. Crystallogr.* **46** 544

[28] Kayanuma K, Kawamura R, Hiramatsu H, Yanagi H, Hirano M, Kamiya T and Hosono H 2008 *Thin Solid Films* **516** 5800

[29] Kamihara Y, Watanabe T, Hirano M and Hosono H 2008 *J. Am. Chem. Soc.* **130** 3296

[30] Guo K, Man Z Y, Wang X J, Chen H H, Tang M B, Zhang Z J, Grin Y and Zhao J T 2011 *Dalton Trans.* **40** 10007

[31] Takano Y, Komatsuzaki S, Komasaki H, Watanabe T, Takahashi Y and Takase K 2008 *J. Alloys Compd.* **451** 467

[32] Dietl T, Ohno H, Matsukura F, Cibert J and Ferrand D 2000 *Science* **287** 1019

[33] Arrott A 1957 *Phys. Rev.* **108** 1394

[34] Arrott A and Noakes J E 1967 *Phys. Rev. Lett.* **19** 786

[35] Mulder C A M, van Duyneveldt A J and Mydosh J A 1981 *Phys. Rev. B* **23** 1384

[36] Lekshmi P N, Raji G R, Vasundhara M, Varma M R, Pillai S S and Valant M 2013 *J. Mater. Chem. C* **1** 6565

[37] Chen B J, Zhao K, Deng Z, Han W, Zhu J L, Wang X C, Liu Q Q, Frandsen B, Liu L, Cheung S, Ning F L, Munsie T J S, Medina T, Luke G M, Carlo J P, Munevar J, Uemura Y J and Jin C Q 2014 *Phys. Rev. B* **90** 155202

[38] Matsukura F, Sawicki M, Dietl T, Chiba D and Ohno H 2004 *Physica E* **21** 1032

[39] Dietl T 2008 *J. Phys. Soc. Jpn.* **77** 031005

[40] Liu X F, Matsuishi S, Fujitsu S, Ishigaki T, Kamiyama T and Hosono H 2012 *J. Am. Chem. Soc.* **134** 11687

[41] Sawicki M, Dietl T, Kossut J, Igalson J, Wojtowicz T and Plesiewicz W 1986 *Phys. Rev. Lett.* **56** 508

[42] Zhang R F, Xu C C, Fu L C, Gu Y L, Zhi G X, Dong J O, Zhao X Q, Xie L F, Zhang H J, Cao C and Ning F L 2022 *J. Magn. Magn. Mater.* **554** 169276